

DOI: 10.1002/adma.200601561

# Variable-Focus Liquid Microlenses and Microlens Arrays Actuated by Thermoresponsive Hydrogels\*\*

By Liang Dong, Abhishek K. Agarwal, David J. Beebe, and Hongrui Jiang\*

Traditional optical systems utilize mechanical parts (e.g., gears, motors, and drivers) to allow adjustable focusing and magnification. Emerging variable-focus microlenses have exhibited the potential to miniaturize and advance optical systems without the need for mechanical parts, impacting significantly on a multitude of fields, such as cameras,<sup>[1]</sup> biomedical instruments,<sup>[2]</sup> and lab-on-a-chip systems.<sup>[3]</sup> A variety of variable-focus liquid microlenses have been demonstrated based on different mechanisms, including reorientation of liquid crystals,<sup>[4]</sup> electrowetting of a liquid droplet,<sup>[1,5]</sup> and mechanical actuation of polymeric materials.<sup>[3,6]</sup> These microlens technologies rely on external controls and power supplies; for example, additional electric fields are necessary to drive both electrowetting liquid microlenses and liquid-crystal microlenses, and external actuation devices are required to control the pressure in flexible polymer microlenses. The requirement for additional discrete components increases the complexity and makes integration, especially in lab-on-a-chip applications, challenging.

We are interested in taking advantage of smart materials to realize variable-focus liquid microlenses without requiring external controls and power supplies. Responsive hydrogels are smart materials that undergo significant and reversible volume change in response to environmental stimuli by absorbing and releasing water through the network interstitials of the hydrogels.<sup>[7]</sup> The ability to convert chemical energy directly into mechanical work means that the hydrogels can function as sensors, actuators, and power sources in specific conditions (e.g., the human body) where most external con-

trols and power supplies are limited or difficult to obtain.<sup>[8]</sup> By taking advantage of responsive hydrogels, we previously reported an innovative approach for realizing smart-liquid microlenses responsive to environmental changes.<sup>[9]</sup> The liquid microlens extends the concept of pinned liquid/liquid interfaces<sup>[10,11]</sup> to apertures to form a liquid microlens. A hydrogel ring located within a microfluidic channel responds to an environmental change by expanding and contracting, which regulates the shape of a water/oil interface (i.e., a liquid microlens), thus, tuning the focal length of the microlens. In this paper, we demonstrate thermoresponsive variable-focus cylindrical microlenses and spherical microlens arrays formed using liquid/liquid interfaces. Thermoresponsive reversible *N*-isopropylacrylamide (NIPAAm) hydrogels were employed; unconstrained NIPAAm hydrogels swell by as much as a factor of ten when the temperature decreases from above to below the hydrogel's lower critical solution temperature (LCST).<sup>[12]</sup> First, arbitrary shapes of microlenses (e.g., cylindrical and spherical) can be realized by patterning apertures that have corresponding shapes (e.g., rectangular and circular, respectively). This benefits the implementation of various microlenses with different shapes, among which variable-focus cylindrical lenses are of strong interest for a multitude of optical applications such as stretching an image, focusing light into a slit, and correcting low-order aberration.<sup>[13]</sup> Second, we extended single variable-focus spherical microlenses to microlens arrays, allowing the devices not only to have wide-angle observation and parallel optical signal acquisition, but also to implement combinatorial interrogation of complicated environments in microfluidics by individually regulating the focal lengths of the microlens elements.

In a typical variable-focus cylindrical microlens (Fig. 1a), a rectangular window was photopatterned in a 250  $\mu\text{m}$  thick polymer slip to form an aperture. The sidewall of the aperture was treated to be hydrophilic (water contact angle of 29°) through an oxygen plasma treatment; the top-side surface of the aperture was rendered hydrophobic (water contact angle of 118°) by coating it with an octadecyltrichlorosilane solution. Thus, a hydrophobic/hydrophilic contact line coincided at the boundary between the sidewall and top-side surface of the aperture. A thermoresponsive NIPAAm hydrogel (LCST = 32 °C) ring was photopatterned in a 750  $\mu\text{m}$  deep microfluidic channel. When the hydrogel ring was filled with deionized water through the aperture, a water meniscus emerged from the rectangular aperture, and the peripheral boundary of the meniscus was pinned stably at the hydrophobic/hydrophilic contact line. Mineral oil was stored within a

[\*] Prof. H. Jiang, Dr. L. Dong, Dr. A. K. Agarwal<sup>[+]</sup>  
Department of Electrical and Computer Engineering  
University of Wisconsin-Madison  
1415 Engineering Drive, Madison, WI 53706 (USA)  
E-mail: hongrui@engr.wisc.edu

Prof. D. J. Beebe  
Department of Biomedical Engineering  
University of Wisconsin-Madison  
1550 Engineering Drive Madison, WI 53706 (USA)

[+] Present address: Biomedical Engineering Department, Northwestern University, 2145 Sheridan Road, Evanston, IL 60208, USA.

[\*\*] This research was partly supported by the U.S. Department of Homeland Security (Grant number N-00014-04-1-0659), through a grant awarded to the National Center for Food Protection and Defense at the University of Minnesota, and was partly supported by Wisconsin Alumni Research Foundation (WARF). Supporting Information is available online from Wiley InterScience or from the author.

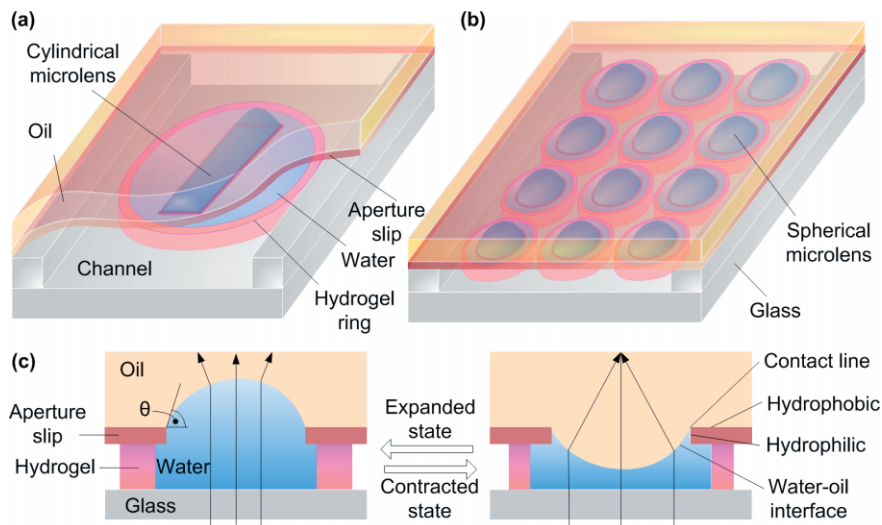


**Figure 1.** a) A schematic of a variable-focus cylindrical liquid microlens. A rectangular aperture was patterned in an aperture slip. A cylindrical microlens was formed using a liquid/liquid interface between oil and water. The water/oil interface was pinned stably at a hydrophobic/hydrophilic contact line shown in (c) along the aperture. A thermoresponsive hydrogel ring was located within a microfluidic channel. When the local environmental temperature increased (decreased), the hydrogel ring contracted (expanded) by releasing (absorbing) water; a resultant net volume change between the hydrogel and water brought about a change in the curvature of the water/oil interface. b) A schematic of a variable-focus spherical liquid microlens array. An array of thermoresponsive hydrogel rings were photopatterned underneath an array of circular apertures. Each spherical liquid microlens was controlled by the same mechanism as the cylindrical lens. c) As the refractive index of oil (1.48) is larger than that of water (1.33), an upward-protruding microlens diverged light (left), whereas a downward bowing microlens converged light (right).

polymer fence to prevent water evaporation. The aperture was 1 mm wide and 4 mm long. As the water meniscus was confined by the aperture, the shape of the microlens followed the shape of the aperture, which was observed to be nearly cylindrical in the central lengthwise (2.5–3.0 mm) section of the rectangular aperture.

As the local environmental temperature changed, the physical volume change of a NIPAAm hydrogel was greater than a correspondingly opposite volume change of a water droplet in the middle of the hydrogel ring,<sup>[9]</sup> and the resultant net volume change of the hydrogel–water system ( $\Delta V_{\text{net}}$ ) induced changes in shape and focal length of the cylindrical microlens. The measured maximum  $\Delta V_{\text{net}}$  of this cylindrical microlens was  $|\Delta V_{\text{net}}|_{\text{max}} = 1.9 \mu\text{L}$  at 43 °C over a tested temperature range of 21–43 °C. The initial volume ( $V_{\text{init}}$ ) of the water meniscus (the volume defined by the rectangular aperture and the water/oil interface) was 1.0  $\mu\text{L}$ , resulting in a starting focus length of –3.3 mm (divergent) at 21 °C. To simulate a change in environmental temperature, a small heater was adhered to the back side of the device. As the temperature increased (decreased), the hydrogel ring contracted (expanded), and the microlens bowed downward (bulged upward). Given a change in temperature, the liquid meniscus stabilized after initially experiencing a small fluctuation. The focal length of the microlens varied from –3.3 mm to  $-\infty$  and from  $+\infty$  to 10.2 mm from 21 to 43 °C, with a divergent to convergent transition point around 33–35 °C (Fig. 2c). The response time

was observed to be around 18 s, referring to the time from activating the heater to a visual change in the shape of the microlens. It is interesting to note that for a given temperature range,  $|\Delta V_{\text{net}}|_{\text{max}}$  and  $V_{\text{init}}$  have a joint effect on the focal-length tuning range. The transformation of the microlens from divergent to convergent could occur if  $0 < V_{\text{init}} < |\Delta V_{\text{net}}|_{\text{max}}$ . This suggests that by controlling the amount of water in the hydrogel ring, the transition point can be arbitrarily set as desired for a specific application.

By responding to a change in environmental temperature, the cylindrical microlens had the ability to focus and shape a laser beam (Fig. 2d). A circular laser beam was incident on the center of the meniscus along the optical axis of the device. A charge-coupled device (CCD) camera coupled to a microscope tracked the image produced by the microlens. The image plane of the microlens was fixed. As the temperature changed from 21 to 43 °C, the focal length of the cylindrical microlens changed, and the output image reached the sharpest line at 38 °C. This observa-

tion indicated that the cylindrical microlens could focus the light in one dimension and could be used to stretch an image.

We have also developed variable-focus liquid spherical microlens arrays responsive to environmental temperatures by using NIPAAm hydrogels (Fig. 1b). Two types of microlens arrays were designed. The type A microlens array incorporated the same NIPAAm hydrogel (LCST = 32 °C) into all of the microlens elements (Fig. 3a), and was fabricated through the same process as a single spherical microlens, but with different photomask patterns. In the type B microlens array (Fig. 4a), we used two NIPAAm hydrogels that had different LCSTs (LCST<sub>1</sub> = 32 °C and LCST<sub>2</sub> = 48 °C) and thus behaved differently when they were exposed to the same environmental temperature. Adjusting the LCST of the second NIPAAm hydrogel was realized by incorporating a small amount of an ionizable monomer (3-(methacryloylamino)propyl trimethylammonium chloride, MAPTAC) into the hydrogel's network.<sup>[14]</sup> Two separate photolithographic steps were needed to photopattern the two types of hydrogels. In both microlens arrays, all lens elements were located in a single microfluidic channel with identical structures.

Figure 3b shows that in the type A microlens array, each element was able to individually adjust its focal length by responding to the local environmental temperature. Initially, all the elements had the same shape at room temperature. When one element (circled) was heated to 43 °C by using a small heater adhered to the underside, the microlens meniscus was

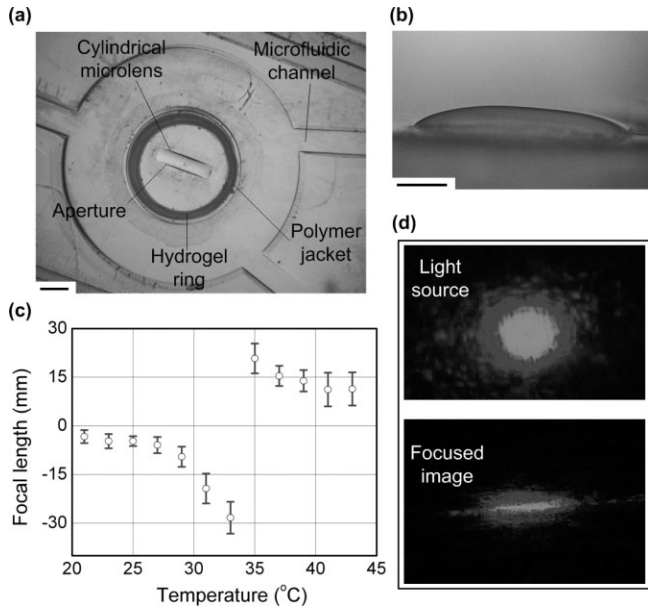


**Figure 2.** a) An optical photograph of a variable-focus cylindrical microlens sensitive to environmental temperature. The polymer jacket was photopatterned around the hydrogel ring to prevent leakage. The scale bar is 2.0 mm. b) A water meniscus of the cylindrical microlens. The scale bar is 1.0 mm. c) The focal length of the microlens as a function of the temperature. The focal length transitioned from a negative to a positive value at around 33–35 °C. The error bars shown are the standard deviation. d) The focusing and shaping of a circular laser beam. The beam was incident along the optical axis of the microlens. Images were observed through a microscope that was coupled to a CCD camera. The image plane of the microlens (i.e., the object plane of the microscope) was fixed during the experiment. Initially, the microscope did not focus the image produced by the microlens. The local temperature was increased, and the image of the circular laser beam became a line at 38 °C because of the change in the focal length.

observed to bow downward. Decreasing the temperature, in turn, caused the meniscus to protrude upward (not shown). The array could also regulate the focal lengths row by row (Fig. 3c). Two heaters separately controlled the temperatures of the two rows. The elements in each row were found to vary their meniscus shapes in response to the changing temperature. We also studied the uniformity of the array. The device was maintained at 35 and 43 °C, respectively, on a hotplate. The height of each element apex was measured using a goniometer. The resulting variation in height at 35 and 43 °C was found to be 8.5 and 11.4 %, respectively. The uniformity could be improved by optimizing device designs and fabrication processes.

The type B microlens array demonstrated that, by utilizing different hydrogels with respective LCSTs, the focal length of each individual lens element was tuned differently when exposed to the same environmental temperature change (Fig. 4). The microlens elements in the front and back rows had  $LCST_1 = 32$  °C and  $LCST_2 = 48$  °C, respectively (Fig. 4a). Figure 4b shows focal lengths of microlens elements as a function of temperature. The response times of both rows were ap-

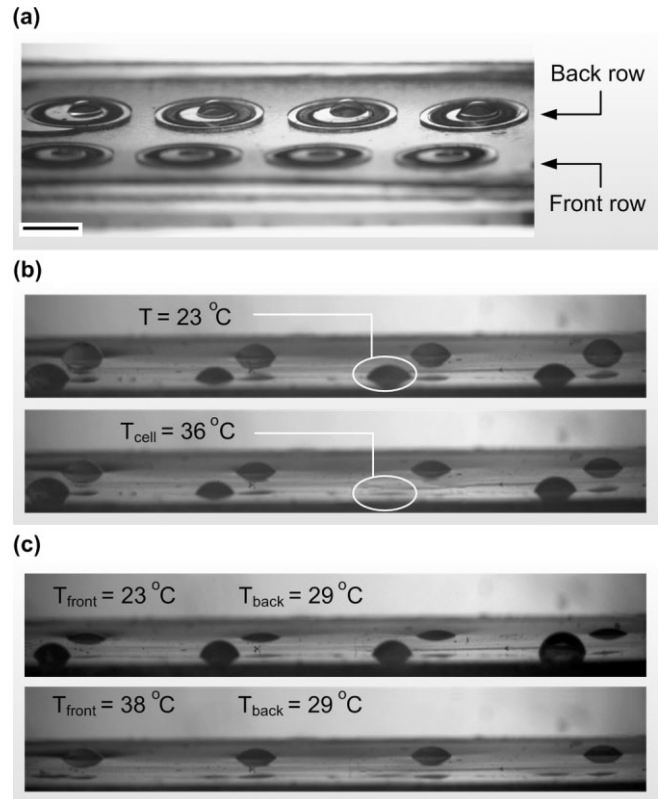


**Figure 3.** a) An optical photograph of the type A variable-focus spherical microlens arrays (2 × 4). All microlens elements in the array used one thermoresponsive hydrogel with a  $LCST = 32$  °C. The scale bar is 2.0 mm. b) The control of an individual element in a microlens array. A small heater was adhered to the back side of the element studied (circled). The element was initially maintained at 23 °C. When the element was heated to 36 °C, it bowed downward. c) The control of the microlens array row by row. The temperatures of the front and back rows ( $T_{front}$  and  $T_{back}$ ) were controlled by two individual heaters.

proximately 20 s. As shown in Figure 4c, all the elements started with the same shape, protruding upward at room temperature. As the temperature increased, the elements in both rows bowed down, but at different rates, thus achieving different focal lengths.

Through spatial scanning, each element in a microlens array was able to image objects in an assigned space onto a predetermined image plane, leading to a parallel acquisition of optical signals and wide-field imaging. Owing to the smartness of thermoresponsive hydrogels, the microlens arrays described above are also applicable to sensing local environmental temperatures. When a distributive temperature exists in microfluidics, the focus of each element can change individually according to the temperature distribution. The optical readout (e.g., change in focal length, light intensity, or image pattern) can be directly related to the profile of the temperature in the microfluidic environment. The use of multiple hydrogels with different LCSTs makes it feasible to program the response of each individual element, allowing flexibility in the design of microlens devices. Furthermore, to implement the sensing of multienvironmental parameters (temperature,<sup>[12]</sup> pH,<sup>[15]</sup>

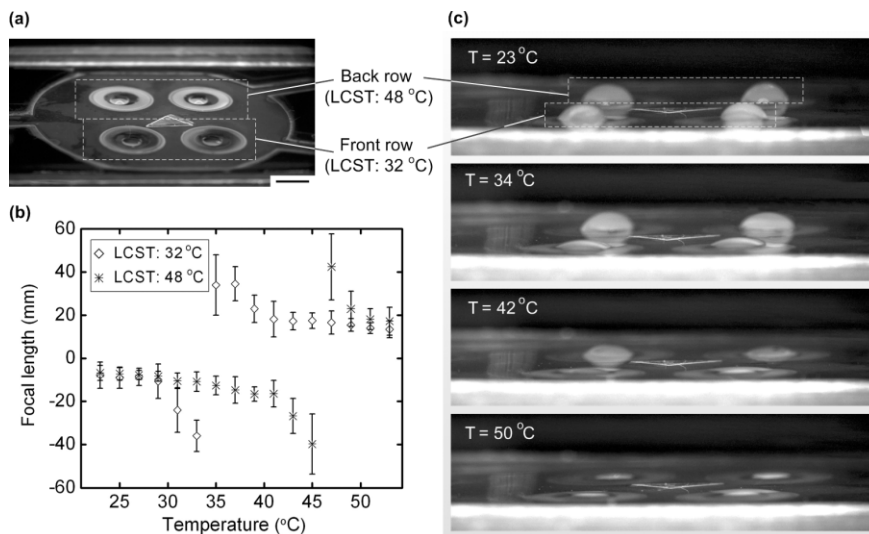


**Figure 4.** a) An optical photograph of the type B variable-focus spherical microlens arrays (2 × 2). The two elements in the front row use LCST<sub>1</sub> = 32 °C and those two in the back row use LCST<sub>2</sub> = 48 °C hydrogels. Small triangular adhesive tape spacers prevented the aperture slips from bending downward during the fabrication of the device. The scale bar is 2.0 mm. b) Focal lengths of the elements with LCST<sub>1</sub> = 32 °C and LCST<sub>2</sub> = 48 °C hydrogels, respectively, as a function of temperature. The error bars shown are the standard deviation. c) The response of the microlens array to varying temperatures. The device was placed on a hotplate. At 23 °C, all the elements were protruding out of the aperture. At 34 °C, slightly over the front row hydrogel's LCST, the front two elements bowed downward significantly, whereas the back two elements bowed downward slightly. At 42 °C, the front two lens elements were convergent (not visible from this angle). At 50 °C, the back two elements began to bow down significantly.

light,<sup>[16]</sup> electric field,<sup>[17]</sup> antigen,<sup>[18]</sup> and glucose<sup>[19]</sup>, a variety of responsive hydrogels can be incorporated into microlens arrays. Each specific environmental parameter can be monitored by one microlens element or a group of elements. Also, the microlens attributes (e.g., microlens shape) can be modified to match specific application needs for optical readouts (e.g., converge light on a line-scanning detector by using a cylindrical microlens). Thus, by appropriately arraying the microlens elements, the microlens technology may provide an interesting approach to sensing biological and chemical agents.

The response times of the microlens devices presented here are of the order of seconds. A faster response is possible by reducing the size of hydrogel structures.<sup>[20]</sup> The down-scaling of the hydrogel size can lead to dense microlens arrays mimicking thousands of repeating microlens units such as those in an insect's compound eyes. The tunability of our microlens elements enables scanning of objects at different distances, providing functionality beyond nature's abilities. The significant advantages of microlens devices described here are that they respond self-adaptively to environmental parameters, thus bypassing the need for complicated external control systems and even power supplies, and that they have the potential to function as sensors to sense complicated parameters. In addition, integration of the microlens devices with microfluidic components (i.e., channels, wells, mixers, and valves)<sup>[21]</sup> is possible through liquid-phase photopolymerization, allowing

the implementation of functionally complex microsystems to advance physical/chemical/biological sensing, photonics, and lab-on-chip technologies.

## Experimental

NIPAAm thermoresponsive hydrogel (LCST = 32 °C) precursor consists of 0.545 g NIPAAm, 0.031 g *N,N'*-methylenebisacrylamide, 0.75 mL dimethyl sulphoxide, 0.25 mL deionized water, and 0.0385 g 2,2-dimethoxy-2-phenylacetophenone (DMPA). To adjust the LCST of the NIPAAm hydrogel to 48 °C, 0.0265 mL of an ionizable monomer, MAPTAC was mixed into the above precursor solution. Aperture slips, microfluidic channels and jackets were prepared by photopatterning poly(IBA) precursor solutions that consist of 1.9 mL isobornyl acrylate (IBA), 0.1 g tetraethylene glycol dimethacrylate, and 0.06 g DMPA.

The devices were fabricated by utilizing liquid-phase photopolymerization based on UV photolithography [20] (see Supporting Information for a schematic of the fabrication process flow). Fabrication started with a polycarbonate cartridge (HybriWells, Grace Bio-Labs, Bend, OR, USA) that was adhered to a liner using an adhesive gasket. The cartridge was first filled with the poly(IBA) precursor mixture. Apertures were formed inside the cartridge using direct photopatterning of the precursor mixture (UV intensity  $I_{UV,poly(IBA)} = 7.7 \text{ mW cm}^{-2}$ ; exposure time  $t_{UV,poly(IBA)} = 24 \text{ s}$ ) and subsequent development in ethanol for 10 s. The liner was subsequently removed and the cartridge was flipped over. An oxygen plasma treatment was then carried out to render sidewalls of the apertures hydrophilic by using a reactive ion-etching system (Technics Micro-RIE series 800-IIC; power supply 70 W at 13.56 MHz; oxygen flowrate 3.0 sccm; gas pressure 107 mtorr; 1 torr = 133.322 Pa; treatment time 10 s). Next, the cartridge was removed and a cavity was formed by adhering the remaining poly(IBA) aperture slip to a glass substrate using double-sided adhesive tape spacers. Poly(IBA) channels and jackets, and NIPAAm hydrogels were photopatterned inside the cavity ( $I_{UV,poly(IBA)} = 8.5 \text{ mW cm}^{-2}$  and  $t_{UV,poly(IBA)} = 34.5 \text{ s}$ ; LCST = 32 °C NIPAAm hydrogel,  $I_{UV,32} = 12.5 \text{ mW cm}^{-2}$  and  $t_{UV,32} = 8.5 \text{ s}$ ; LCST = 48 °C NIPAAm hydrogel,  $I_{UV,48} = 15 \text{ mW cm}^{-2}$  and  $t_{UV,48} = 10 \text{ s}$ ). Then, the top-side surface of the aperture slip was treated as hydrophobic by carefully brushing onto it an octadecyltrichlorosilane solution (OTS, diluted by hexadecane (0.2 vol%)) without affecting the side walls of the apertures. Finally, a polydimethylsiloxane (PDMS) elastomer fence, bonded with a glass cover slip, was glued to the aperture slip. The microlens liquids (water and mineral oil) were introduced into the device through a hole drilled in the glass cover slip.

We then measured the focal length of the convergent microlenses at different temperatures. A collimated laser beam (670 nm) was incident on the microlens from one side; the output beam was collected by a microscope coupled to a CCD camera at the other side. The microscope was first focused at the top-side surface of the aperture. Then, the sample stage was moved so that the microscope focused the image produced by the microlens. The distance the stage traveled was thus the focal length of the microlens. For divergent microlenses, we first measured the angle  $\theta$  (see Fig. 1c) of the water/oil interface to

the top-side surface of the aperture using a goniometer. The focal length was calculated using the equation  $f = -n_1 r ((n_1 - n_2) \sin \theta)^{-1}$ , where  $f$  is the focal length,  $n_1$  and  $n_2$  are the refractive index of mineral oil ( $n_1 = 1.48$ ) and water ( $n_2 = 1.33$ ), and  $r$  is the radius of the aperture.

Received: July 12, 2006

Revised: November 10, 2006

Published online: January 11, 2007

- 
- [1] S. Kuiper, B. H. W. Hendriks, *Appl. Phys. Lett.* **2004**, *85*, 1128.
- [2] K. Carlson, M. Chidley, K. B. Sung, M. Descour, A. Gillenwater, M. Follen, R. Richards-Kortum, *Appl. Opt.* **2005**, *44*, 1792.
- [3] N. Chronis, G. L. Liu, K. H. Jeong, L. P. Lee, *Opt. Express* **2003**, *11*, 2370.
- [4] G. Li, D. L. Mathine, P. Valley, P. Ayras, J. N. Haddock, M. S. Giridhar, G. Williby, J. Schwiegerling, G. R. Meredith, B. Kippelen, S. Honkanen, N. Peyghambarian, *Proc. Natl. Acad. Sci. USA* **2006**, *103*, 6100.
- [5] S. Yang, T. N. Krupenkin, P. Mach, E. A. Chandross, *Adv. Mater.* **2003**, *15*, 940.
- [6] D. Y. Zhang, V. Lien, Y. Berdichevsky, J. Choi, Y. H. Lo, *Appl. Phys. Lett.* **2003**, *82*, 3171.
- [7] Y. Osada, J. P. Gong, Y. Tanaka, *J. Macromol. Sci. Polym. Rev.* **2004**, *44*, 87.
- [8] Y. Osada, J. Gong, *Prog. Polym. Sci.* **1993**, *18*, 187.
- [9] L. Dong, A. K. Agarwal, D. J. Beebe, H. Jiang, *Nature* **2006**, *442*, 551.
- [10] B. Zhao, J. S. Moore, D. J. Beebe, *Science* **2001**, *291*, 1023.
- [11] J. Atencia, D. J. Beebe, *Nature* **2005**, *437*, 648.
- [12] J. Wang, Z. Chen, M. Mauk, K. S. Hong, M. Li, S. Yang, H. H. Bau, *Biomed. Microdevices* **2005**, *7*, 313.
- [13] Y. H. Lin, H. W. Ren, K. H. Fan-Chiang, W. K. Choi, S. Gauza, X. Y. Zhu, S. T. Wu, *Jpn. J. Appl. Phys.* **2005**, *44*, 243.
- [14] H. van der Linden, W. Olthuis, P. Bergveld, *Lab Chip* **2004**, *4*, 619.
- [15] T. G. Park, A. S. Hoffman, *J. Appl. Polym. Sci.* **1992**, *46*, 659.
- [16] A. Suzuki, T. Tanaka, *Nature* **1990**, *346*, 345.
- [17] T. Tanaka, I. Nishio, S. T. Sun, S. Uenonishio, *Science* **1982**, *218*, 467.
- [18] T. Miyata, N. Asami, T. Urugami, *Nature* **1999**, *399*, 766.
- [19] A. Guiseppi-Elie, S. I. Brahim, D. Narinesingh, *Adv. Mater.* **2002**, *14*, 743.
- [20] D. J. Beebe, J. S. Moore, J. M. Bauer, Q. Yu, R. H. Liu, C. Devadoss, B. H. Jo, *Nature* **2000**, *404*, 588.
- [21] A. K. Agarwal, S. S. Sridharamurthy, D. J. Beebe, H. Jiang, *J. Microelectromech. Syst.* **2005**, *14*, 1409.
-